Journal of Colloid and Interface Science 601 (2021) 678–688

Contents lists available at ScienceDirect

Journal of Colloid and Interface Science

journal homepage: www.elsevier.com/locate/jcis

Regular Article

Cellulose nanocarriers via miniemulsion allow Pathogen-Specific agrochemical delivery

Thiago O. Machado [a,b], Sebastian J. Beckers [a], Jochen Fischer [c], Claudia Sayer [b], Pedro H.H. de Araújo [b], Katharina Landfester [a], Frederik R. Wurm [a,d,*]

[a] Max Planck Institute for Polymer Research, Ackermannweg 10, 55128 Mainz, Germany
[b] Department of Chemical Engineering and Food Engineering, Federal University of Santa Catarina, PO Box 476, Florianópolis, SC 88040 900, Brazil
[c] Institute for Biotechnology and Drug Research, Erwin-Schrödinger-Str. 56, 67663 Kaiserslautern, Germany
[d] Sustainable Polymer Chemistry Group, Department of Molecules and Materials, MESA+ Institute for Nanotechnology, Faculty of Science and Technology, Universiteit Twente, PO Box 217, 7500 AE Enschede, the Netherlands

GRAPHICAL ABSTRACT

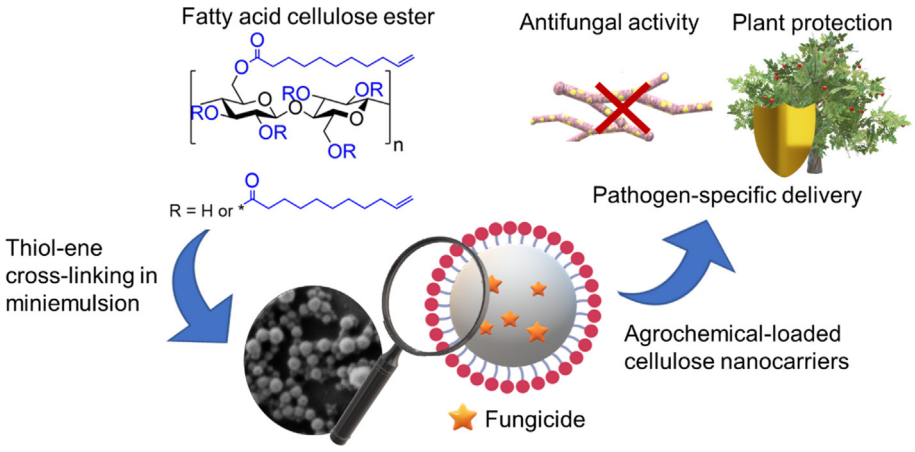

ARTICLE INFO

Article history:
Received 21 December 2020
Revised 20 April 2021
Accepted 6 May 2021
Available online 14 May 2021

Keywords:
Cellulose nanocarriers
Drug delivery in plants
Thiol-ene addition
Miniemulsion
Sustainable agriculture
Crop protection

ABSTRACT

The current spraying of agrochemicals is unselective and ineffective, consuming a high amount of fungicides, which endangers the environment and human health. Cellulose-based nanocarriers (NCs) are a promising tool in sustainable agriculture and suitable vehicles for stimuli-responsive release of agrochemicals to target cellulase-segregating fungi, which cause severe plant diseases such as Apple Canker. Herein, cellulose was modified with undec-10-enoic acid to a hydrophobic and cross-linkable derivative, from which NCs were prepared via thiol-ene addition in miniemulsion. During the crosslinking reaction, the NCs were loaded *in situ* with hydrophobic fungicides, Captan and Pyraclostrobin. NCs with average sizes ranging from 200 to 300 nm and an agrochemical-load of 20 wt% were obtained. Cellulose-degrading fungi, e.g. *Neonectria. ditissima* which is responsible for Apple Canker, lead to the release of fungicides from the aqueous NC dispersions suppressing fungal growth. In contrast, the non-cellulase segregating fungi, e.g. *Cylindrocladium buxicola*, do not degrade the agrochemical-loaded NCs. This selective action against Apple Canker fungi, *N. ditissima*, proves the efficacy of NC-mediated drug delivery triggered by degradation in the exclusive presence of cellulolytic fungi. Cellulose NCs represent

* Corresponding author at: Sustainable Polymer Chemistry Group, Department of Molecules and Materials, MESA+ Institute for Nanotechnology, Faculty of Science and Technology, Universiteit Twente, PO Box 217, 7500 AE Enschede, the Netherlands.
E-mail address: frederik.wurm@utwente.nl (F.R. Wurm).

https://doi.org/10.1016/j.jcis.2021.05.030
0021-9797/

a sustainable alternative to the current unselective spraying of agrochemicals that treats many crop diseases ineffectively.

1. Introduction

Only about 10% of the over 4 million tonnes of pesticides applied annually to fields worldwide reach the targeted crop, due to poor uptake, runoff, and degradation [1-3]. This off-target application of pesticides generates grave environmental problems and poses risk to human health; therefore, it is essential to achieve sustainable crop production while maintaining crop yield [4].

Stimuli-responsive nanocarriers (NCs) for triggered release of agrochemicals have the potential to reduce environmental impact while the volume of agricultural production remains unaltered [5,6]. We have prepared cellulose NCs with high agrochemical-load that can be selectively cleaved by cellulases from plant pathogens, such as the fungal disease Apple Canker. The fungi secrete enzymes to destroy plant tissue containing cellulose to collect nutrients. Agrochemical-loaded NCs designed from the nutrient source of the fungi are degraded by fungal enzymes and, thereby, release actives at the site of the infection.

Our previous work used lignin NCs relying on triggered release by lignin-degrading fungi, [7,8] but several plant pathogens use cellulose as a nutrient source, such as the fungus *Neonectria ditissima (syn. Nectria galligena)*, responsible for causing European Canker (Apple Canker), a disease with no curative treatment available, leading production losses of many fruit crops worldwide, remarkably affecting apple trees [9-11]. For this reason, cellulose nanocarriers are promising vehicles for the pathogen-specific delivery of agrochemicals against cellulase-segregation fungi. The design of cellulose-based NCs for cellulase triggered the release of fungicides has not yet been investigated. In such a delivery system, the disease-associated fungi degrade the loaded cellulose NCs and fungicide is released exclusively at the site of infection, which allows preventive and curative treatment (Scheme 1).

NCs based on cellulose derivatives, e.g. carboxymethyl cellulose, have been reported in few cases for agrochemical delivery; however, the agrochemical load reported was low (<8%) and the delivery was based on diffusive release only [12]. To prepare NCs with high agrochemical load, the miniemulsion technique can be used, in which the hydrophobic fungicide and the monomer or pre-formed polymer are dispersed in a continuous aqueous phase; then the encapsulation of the fungicide and the formation of polymer NCs occur in one single step. To that end, we needed a common solvent able to dissolve the agrochemicals and the cellulose and form the dispersed phase, which is only possible by chemically modifying cellulose to a hydrophobic derivative. Strategies for its chemical modification allow the development of building blocks for nanostructures [13-15]. Cellulose was chemically modified with fatty acid chains, namely undec-10-noic acid, to produce an organo-soluble ester derivative with pendant double bonds. Subsequently, covalently crosslinked NCs were prepared in miniemulsion via thiol-ene addition of cellulose undecenoate with a dithiol, DL-dithiothreitol, followed by solvent evaporation. Captan and Pyraclostrobin, non-systemic and systemic fungicides, respectively, utilized in the field against European Canker, were introduced in the organic phase and encapsulated *in situ* during the miniemulsion step. The miniemulsion technique allows the formation of aqueous NC dispersions that can be readily utilized; thus, the as-synthesized dispersions were studied *in vitro* to evaluate their antifungal activity. Dose-dependent tests determined the minimum inhibitory concentration (MIC) of NCs formulations towards several pathogens. Furthermore, the inhibition effects of agrochemical-loaded cellulose NCs on germination and mycelial growth of European Canker pathogen and non-cellulolytic fungus were compared, and nanoformulations were only active in the presence of cellulase-segregating fungi due to the degradation-triggered release of fungicides. This strategy represents a more sustainable alternative to the current unselective spraying of agrochemicals that treats many crop diseases ineffectively.

2. Experimental section

2.1. Materials

Sigmacell Cellulose type 20, undec-10-enoic acid (98%), DL-dithiothreitol (DL-DTT, ≥ 98%), lithium chloride, 2-chloro-4,4,5,5-tetramethyl-1,3,2-dioxaphospholane (95%), 1,8-Diazabicyclo[5.4.0

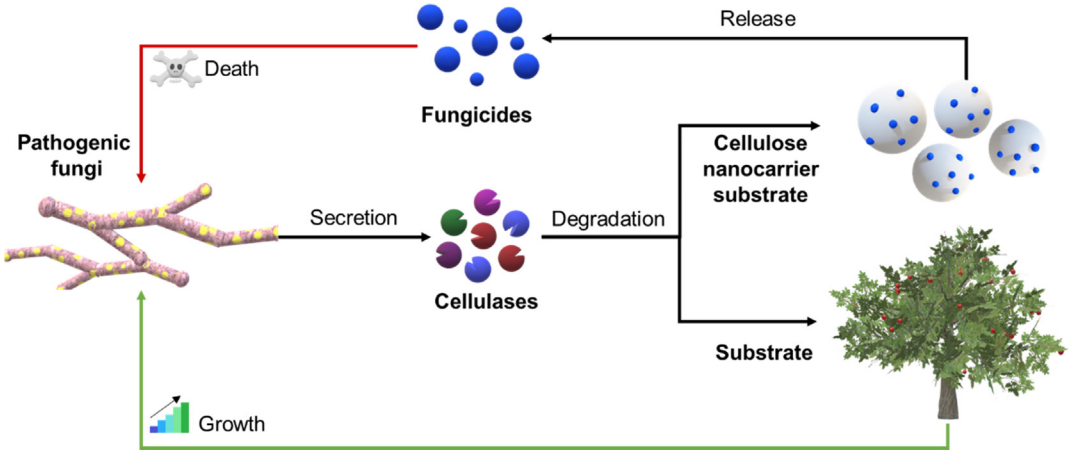

Scheme 1. Concept of the NCs-mediated agrochemical delivery in plants: green pathway: degradation of a substrate inside of the plant leads to the growth of the pathogen and the progress of the infection/disease; red pathway: a negative feedback loop is initiated by concealing a fungicide that fights the pathogen in NCs based on the nutrient source of the pathogen. Fungicide-loaded cellulose NCs release the agrochemical load only in the presence of cellulolytic enzymes secreted by pathogens.

]undec-7-ene (DBU, ≥ 90%), *endo*-*N*-hydroxy-5-norbornene-2,3-di carboximide (*N*-Hydroxy-5-norbornene-2,3-dicarboxylic acid imide, 97%), pyridine (99.8%), deuterated chloroform ($CDCl_3$, 99.96%), potassium persulfate (KPS, ACS reagent, ≥ 99.0%) and chromium(III) acetylacetonate (97%) were purchased from Sigma-Aldrich and used as received. Pyraclostrobin and Captan were purchased from TRC Canada. *N*,*N*-Dimethylacetamide (DMAc, anhydrous, 99.8%) and isopropanol (≥99.5%) were obtained from Merck. The lithium chloride and cellulose were dried at 100 °C in a vacuum oven overnight before use. The anionic surfactant sodium dodecyl sulfate (SDS) was purchased from Alfa Aesar and used as received.

2.2. Esterification of cellulose with Undec-10-enoic acid

Cellulose was modified by esterification with undec-10-enoic acid to produce a fatty acid cellulose ester (UACE). Firstly, undec-10-enoic acid (11.37 g, 61.7 mmol) is reacted with 1,1′-carbonyl diimidazole (CDI, 11 g, 67.8 mmol) in a round-bottom flask using 40 mL of DMAc (37.6 mL) as a solvent. UA is added dropwise under stirring due to the formation of CO_2 upon the coupling with CDI; then, the solution was placed in an oil bath at 50 °C overnight for 15 h to assure the complete conversion of UA to the intermediate acylimidazole, as reported in the literature [16]. Secondly, two grams of cellulose (Sigmacell cellulose type 20) is added to a round-bottom flask containing 100 mL of DMAc/LiCl (7 wt%) and the system is stirred and allowed to form a slurry under argon flow for 10 min; then, the flask is sealed and placed in an oil bath at 160 °C under stirring for 3 h. Finally, after the complete dissolution of cellulose to form a golden solution, the temperature is lowered to 80 °C and the solution containing the intermediate acylimidazole, prepared in the first stage, was added dropwise to the golden cellulose solution. The esterification reaction was carried out for 120 h under stirring (500 rpm) at 80 °C. The reaction mixture was precipitated into isopropanol under vigorous stirring, the solid was isolated by filtration, repeatedly washed with isopropanol thrice and once with water. The product was freeze-dried after purification. Yields are typically from 20 to 50% to native cellulose.

2.3. Preparation of nanocarriers

The preparation of cellulose nanocarriers was carried out by thiol-ene cross-linking in miniemulsion followed by solvent evaporation. The typical procedure is the following: A honey-like solution was formed upon the dispersion of UACE (500 mg) in 15 g of chloroform by vigorous stirring with an Ultra Turrax® homogenizer at 20,000 rpm for 3 min under ice-cooling. The amount of solvent lost during the homogenization was replenished and the final solution was used throughout the experiments. 1.55g of the honey-like UACE solution was added into an aqueous solution (4.5 mL) containing 0.1 wt% of the surfactant SDS and the resulting mixture was pre-emulsified by vigorous stirring using an Ultra Turrax® homogenizer at 20,000 rpm for 1 min under ice-cooling to prevent evaporation of the organic solvent. The pre-emulsion was submitted to ultrasonication for 3 min (1/2 in. tip, 70% amplitude, 20 s pulse on followed by 10 s pulse off) under ice-cooling to prevent evaporation of the solvent. After the formation of a miniemulsion, an aqueous solution (0.5 mL) containing the crosslinker, DTT (25 mg), and the initiator KPS (4.4 mg, 10 mol% to DTT), was added dropwise. After the addition of the crosslinker, the reaction was carried out for 15 h at 50 °C under mild stirring. After the completion of the cross-linking process, chloroform was evaporated by stirring the open vessel overnight at room temperature and the amount of water lost in the process was replenished to complete 5 mL. To encapsulate a set of agrochemicals to treat fungal infections, 10 mg of fungicides, pyraclostrobin, and captan, were introduced in the organic phase together with the UACE and chloroform, and the procedure followed as described above. The final concentration of fungicide was 2 $mg{\cdot}mL^{-1}$ to the volume of latex and 20 wt% to UACE.

2.4. Dynamic light scattering

The hydrodynamic diameters of the particles were measured by DLS with Zetasizer Nano S90 submicron particle sizer (Malvern Panalytical, UK) at a fixed angle of 90° and a laser diode running at 633 nm, samples were diluted before measurement.

2.5. Gel permeation chromatography

For GPC measurements in DMAc (containing 9 wt% of lithium chloride as an additive) an Agilent 1100 Series (Agilent Technologies 1260 Infinity) was used as an integrated instrument, including a PSS GRAM linear M column, a UV detector (270 nm), and a RI detector at a flow rate of 0.5 $mL{\cdot}min^{-1}$ at 80 °C. Calibration was carried out using PS standards provided by Polymer Standards Service.

2.6. Electron microscopy

An LEO Gemini 1530 (Zeiss GmbH, Germany) scanning electron microscope (SEM) was used to visualize the nanocarriers. The dispersion was diluted in water and drop-cast on conductive carbon adhesive tapes resting on a stub. After drying of the SEM sample at room temperature, it was inserted into a sample holder and transferred into the SEM. The SEM was operated at an acceleration voltage of 0.7 kV.

2.7. NMR spectroscopy

^{1}H and ^{31}P nuclear magnetic resonance (NMR) spectroscopy was performed at a Bruker AVANCE (USA) system at 300 MHz. For ^{1}H NMR spectroscopy, 5 mg of the sample was dispersed in 600 μL of $CDCl_3$. To determine the number of OH groups in the sample, ^{31}P NMR spectroscopy was used after derivatization according to the literature [13] for other cellulose derivatives: ca. 25 mg of dried sample was weighed and dissolved in 500 μL of $CDCl_3$. Pyridine (150 μL) was added upon complete dissolution. Afterwards, *endo*-*N*-hydroxy-5-norbornene-2,3-dicarboximide (125 μL, 123.21 mM in Pyridine : $CDCl_3$ / 3 : 2, 0.0154 mmol) as internal standard was added and the solution was stirred for 15 min, then 2-chloro-4,4,5,5-tetramethyl-1,3,2-dioxaphospholane (100 μL, 0.63 mmol) was added to the solution and allowed to stir for 15 min, lastly, a solution of chromium(III) acetylacetonate (50 μL, 50 mM in pyridine : $CDCl_3$ / 3 : 2) as relaxation agent the solution was stirred for further 5 min. Then, 700 μL of the solution was transferred to an NMR tube. DS values were calculated according to the equation discussed in the literature [17] and described below in Eq. (3):

$$DS = DS_{max.} \times \left(\frac{\frac{1}{OH_{free}} - \frac{1}{OH_{cel.}}}{M.W._{\cdot subs.} + \frac{1}{OH_{free}} - 1} \right) \quad (3)$$

Where *DS* is the degree of substitution, $DS_{max.}$ is the maximum degree of substitution per AGU, which is 3, OH_{free} is the number of free hydroxyls in the fatty acid cellulose ester per weight of the sample, $OH_{cel.}$ is the number of hydroxyls in cellulose per weight of anhydroglucose unit (AGU), $M.W._{\cdot subs.}$ is the molecular weight of the fatty acid substituent minus OH (17 $g{\cdot}mol^{-1}$). OH_{free} is calculated based on the ^{31}P NMR spectrum given by Eq. (4):

$$OH_{free} = \frac{[standard] \times I_{OH}}{I_{standard}} \times \frac{1}{M_S} \quad (4)$$

Where I_{OH} is the integral from 140 to 150 ppm of phosphorylated hydroxyl groups in modified cellulose samples, $I_{standard}$ is the integral from 151 to 152 ppm of the phosphorylated dicarboximide standard, and M_S is the weight of the sample. $OH_{cel.}$ is a theoretical value given by Eq. (5):

$$OH_{cel.} = \frac{DS_{max.}}{M.W._{AGU}} \quad (5)$$

Where $DS_{max.}$ is the maximum degree of substitution per AGU, which is 3, and $M.W._{AGU}$ is the molecular weight of an AGU, which is 162.14 g·mol^{-1}.

2.8. IR spectroscopy

To investigate the chemical structures of cellulose, undec-10-enoic acid cellulose ester (UACE), and crosslinked nanocarriers, their Fourier transform infrared (FTIR) spectra were recorded by Nicolet iS10 with Vertical ATR Accessory. Cellulose and fatty acid cellulose esters samples were dried at 50 °C temperature in the vacuum oven overnight, while the nanocarriers were extracted from the latex by centrifugation, at 10,000 rpm for 60 min, washed twice with water to remove any water-soluble impurities, and dried in a vacuum oven at 50 °C overnight. Spectra were recorded between 600 and 4000 cm^{-1} at a resolution of 4 cm^{-1} and codding 32 scans.

2.9. Degree of crystallinity

Huber image plate Guinier camera 670 with a step size 0.02° at 2.5 *sec* step time. Cu radiation = 1.5418 Å, and 2θ = 10 – 70° range, employing a scanning rate of 2.5°/min. The degree of crystallinity was estimated by XRD by a methodology validated in the literature [18], which considers the intensity of crystalline diffraction and the intensity of the amorphous halo as follows in Eq. (6):

$$\text{uCrI}(\%) = \frac{\text{Intensity}(002) - \text{Intensity}(am)}{\text{Intensity}(002)} \times 100\% \quad (6)$$

Where the intensity of crystalline diffraction from plane 002 in cellulose, intensity (002), is obtained at 22.5° and the intensity of the amorphous halo is obtained at 21°.

2.10. Encapsulation efficiency

The encapsulation efficiency was evaluated by two methods: a direct method, which is achieved by quantifying the amount of fungicide enclosed in the NCs, and an indirect method, which consists of measuring the amount of remaining fungicide in the supernatant and calculating, by difference, the encapsulated amount. Latexes were submitted to centrifugation (10,000 rpm for 60 min) and the aqueous supernatant isolated thereof was used to estimate the encapsulation efficiency according to the indirect method. The precipitated NCs were freeze-dried and ca. 5 – 10 mg was placed in a vial with THF under stirring at room temperature for 24 h to extract the encapsulated fungicides, then the NCs were filtered off with a syringe filter (pore size: 450 nm) and the extract was analyzed in by HPLC to provide the encapsulation efficiency by the direct method. The HPLC measurements were performed on an Agilent Technologies Series 1200 setup equipped with a UV detector (pyraclostrobin at 280 nm, captan at 220 nm) and an ELSD detector 385-LC (both Agilent Technologies, USA). The analyses were performed using an Agilent Eclipse Plus C18 and an eluent gradient from THF/water + 0.1% FA 20/80 to 100/0. The encapsulation efficiencies were calculated according to the equations below (direct method, Eq. (7); and indirect method, Eq. (8)):

$$EE(\%) = \frac{m(extractedfungicide)}{m(totalfungicide)} \times 100\% \quad (7)$$

$$EE(\%) = \frac{m(totalfungicide) - m(fungicidesupernatant)}{m(totalfungicide)} \times 100\% \quad (8)$$

The HPLC calibration curved can be found in the Supplementary Material, Figure S1 for captan, and Figure S2 for pyraclostrobin.

2.11. Antifungal activity

Neonectria ditissima (syn. *Neonectria galligena*), *Phaeoacremonium minimum* and *Cylindrocladium buxicola* were used for the spore germination and mycelial growth test as found in the literature [7]. Conidia from 18-day-old agar plate cultures were harvested. After centrifugation at 4000 rpm for 10 min, the conidia were re-suspended in YMG-medium (10 g·L^{-1} malt extract, 10 g·L^{-1} glucose, 4 g·L^{-1} yeast extract, pH 5.5) to a concentration of 10^5 per mL. The test was carried out in 96-well microliter plates (Greiner Bio-One GmbH, Frickenhausen) with conidia in 200 µL of YMG-medium and an incubation time of 96 h at 27 °C The optical density was measured at a wavelength of 600 nm (Benchmark Plus Microplate reader, BioRad, Munich). Tests were conducted in triplicates. The concentration of latexes in the antifungal tests was equivalent to a fungicide concentration of 5 µg per 200 µL (25 mg·mL^{-1}) medium in a well. The spores were diluted in yeast glucose mineral (YMG) medium to a final concentration of 2000 spores·mL^{-1} and added to the nanoparticles in the well to complete 200 µL. The plates were incubated at 27 °C and 120 rpm on an incubator and the optical density (OD) was measured every 24 h at a wavelength of 600 nm. The antifungal activity was obtained by comparing the OD after the incubation of samples treated with the positive control (just water is added), the negative control (hygromycin, 100 mg·mL^{-1}) to assure complete fungal growth inhibition, the nanocarriers dispersion, and the free fungicide. The OD relative to the positive control is considered 100% of fungal growth.

3. Results and discussion

3.1. Undec-10-enoate cellulose esters (UACE)

Cellulose undec-10-enoate was synthesized via esterification of cellulose with undec-10-enoic acid using CDI as the coupling agent (Figure S3). IR spectroscopy of UACE proved the decrease of the –OH stretch band at 3550 – 3400 cm^{-1} in UACE, the advent of bands at 1743 cm^{-1} due to C=O stretch in ester groups, increased vibrations at 2921 and 2851 cm^{-1} due to CH antisymmetric and symmetric stretch from CH_2 and CH_3 of the alkyl chains of undecenoic acid, at 1155 cm^{-1} the C—O—C antisymmetric stretch in aliphatic esters, and at 3075, 1640 and 907 cm^{-1} vibrations for the = C—H and C=C stretch in alkenes, and CH_2 out of plane wag of vinyl compounds (Fig. 1b; FT-IR spectra were normalized to the C—O band from anhydroglucose unit (AGU) at ca. 1050 cm^{-1}).

The degree of functionalization of cellulose was determined by a derivatization method from ^{31}P NMR (Fig. 1a).[17] A degree of substitution, DS = 2.35, was calculated from the ^{31}P NMR spectrum. ^{1}H NMR spectroscopy further proved the successful synthesis of undec-10-enoic acid-modified cellulose (Fig. 1c). Hydrogens relative to the AGU appear from 4.8 to 3.0 ppm; the multiplet relative to hydrogen b in the vinyl moiety is detected at 5.8 ppm, whereas vinylic hydrogens a and a', which interact by geminal coupling, are revealed from 4.8 to 5.1 ppm; the remainders are relative to

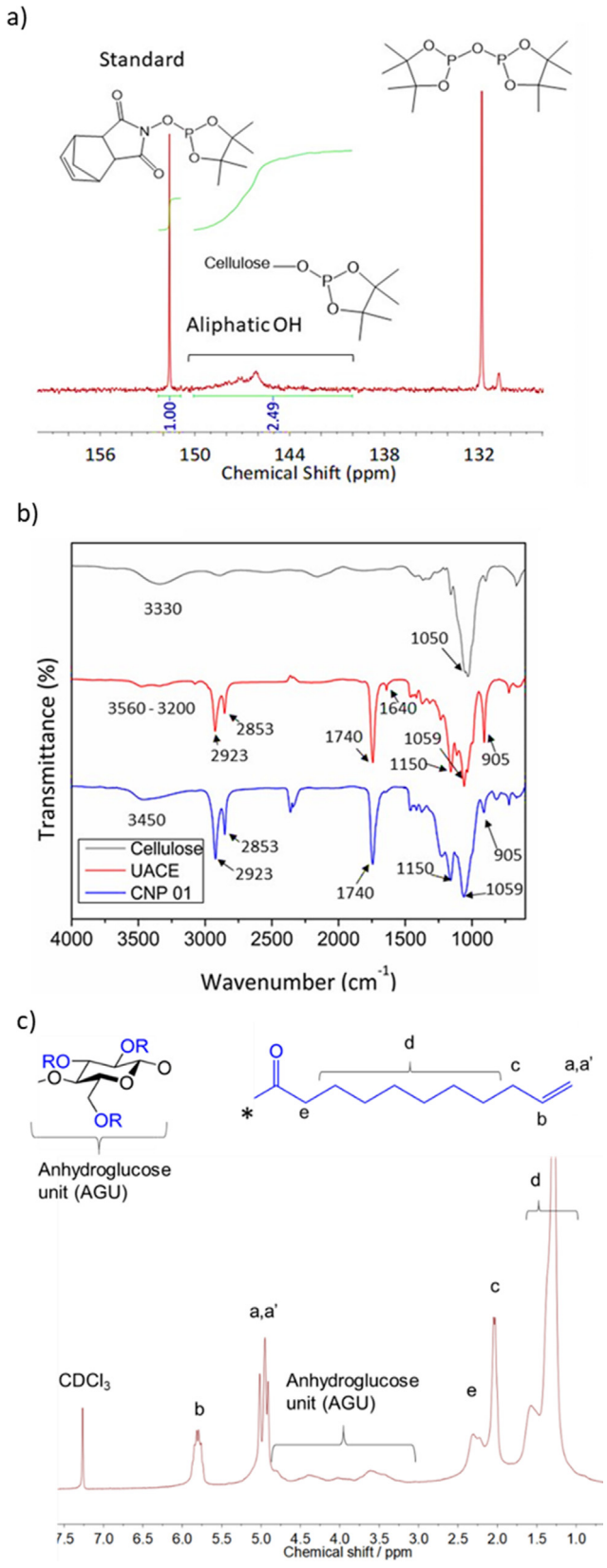

Fig. 1. a) ^{31}P NMR spectra by a process of derivatization of the remaining hydroxyl groups, as phosphite esters, UACE. b) Infrared spectra of native cellulose (gray), UACE (red), and cellulose nanocarriers (blue). The spectra are normalized to the band at 1050–1065 cm^{-1} of C—O of AGU in native cellulose. c) ^{1}H NMR spectrum of UACE with peak assignments. (For interpretation of the references to colour in this figure legend, the reader is referred to the web version of this article.)

methylene groups neighboring a varied electronic environment. The proportion between the integrals of the resonances relative to the hydrogen 'b" bonded to the vinyl carbon and the AGU (Fig. 1c) have shown to be roughly three double bonds or fatty acid chains per AGU, which is a similar DS as determined from the ^{31}P NMR spectra of ca. 2.4.

The molecular weights of cellulose and cellulose ester were determined by GPC (Table 1). The apparent number average molecular weight before chemical modification was found to be 8.2 kDa, whereas UACE exhibited a number average molecular weight of 18.7 kDa (compared to polystyrene (PS) standards). The GPC-results evidence changes in the polymer structure that governs polymer properties in solution. The increase of the apparent molecular weight denotes an increase in the radius of gyration due to the grafting with fatty acid chains rather than precise molecular weights. The used batch of cellulose was a semicrystalline polymer with ca. 40% of crystallinity estimated by XRD. After the esterification with undec-10-enoic acid, an amorphous polymer was obtained (Fig. 2a). Crystallinity index was estimated as described in the literature by considering the crystalline diffraction intensity of the plane (0 0 2) at 22.5° and subtracting the intensity of the amorphous halo at 21° [18]. Fatty acid moieties act as spacer groups in the macromolecular structure, which impedes the hydrogen bonding that bestows the semicrystalline characteristic to cellulose.

Thermogravimetry (TGA) proved similar thermal stability of UACE and the cellulose precursor with 50% of mass loss occurred at 341 or 333 °C, respectively (Fig. 2b). Native cellulose contained a small amount of water, of < 5 wt%; the end of this first decomposition stage is reached at ca. 350 °C with > 70% of mass loss followed by the change in slope and the decomposition of the final 20% residual mass. The second decomposition stage occurs slower in UACE due to the fatty acid esters (Fig. 2b). Onwukamike et al. have obtained similar TGA results regarding the second decomposition stage for fatty acid cellulose esters (DS > 1) obtained by transesterification of cellulose with high oleic sunflower oil [19].

DSC proved that the crystallinity of native cellulose vanished after the modification, with UACE being amorphous up to ca 170 °C (Fig. 2c). The melting temperature of cellulose was determined from the first DSC run at 184 °C. In contrast, the amorphous cellulose ester exhibited an exothermic event upon heating, which might be a melt crystallization at 174 °C (additional DSC data is shown in Figure S4). The fatty acid spacer groups contribute, after chemical modification, to reduce the organization of the polymer chains that must be disentangled. The necessary mobility to disentangle the polymer chains is provided upon heating which promotes the reorganization and the establishment of some crystalline domains [20]. Native cellulose and UACE were submitted to scanning electron microscopy analyses to visualize the modification in the microstructural patterns (Figure S5). Microcrystalline cellulose appears as classic solid grains [21], while UACE seems amorphous, as confirmed by DSC and XRD analyses. The results demonstrate the successful esterification of undec-10-enoic acid with cellulose to an amorphous cellulose-ester, bearing multiple double bonds suitable for thiol-ene crosslinking reactions.

3.2. Nanocarrier preparation

Thiol-ene addition has been reported in the literature as a suitable strategy to produce polymers and nanocarriers from renewable resources, especially to polymerize vegetable oils [22]. Thiol-ene addition is considered as a click reaction since it can be carried out under mild conditions and normally provides high yields and no by-products. Novel biomaterials are arising from thiol-ene polymerization due to the interest in the unique crosslinking structure,

Table 1
Summary of the molecular weights of native cellulose and UACE samples, crystalline indexes, CrI, and degree of substitution (DS).

Entry	M_n* (kDa)	M_w* (kDa)	Đ	CrI (%)	DS
Cellulose	8.2	20.4	2.5	56	–
UACE	18.7	52.9	2.8	–	2.35

* Molecular weights are compared to PS standard and denote a change in polymer structure rather than precise M.W. values.

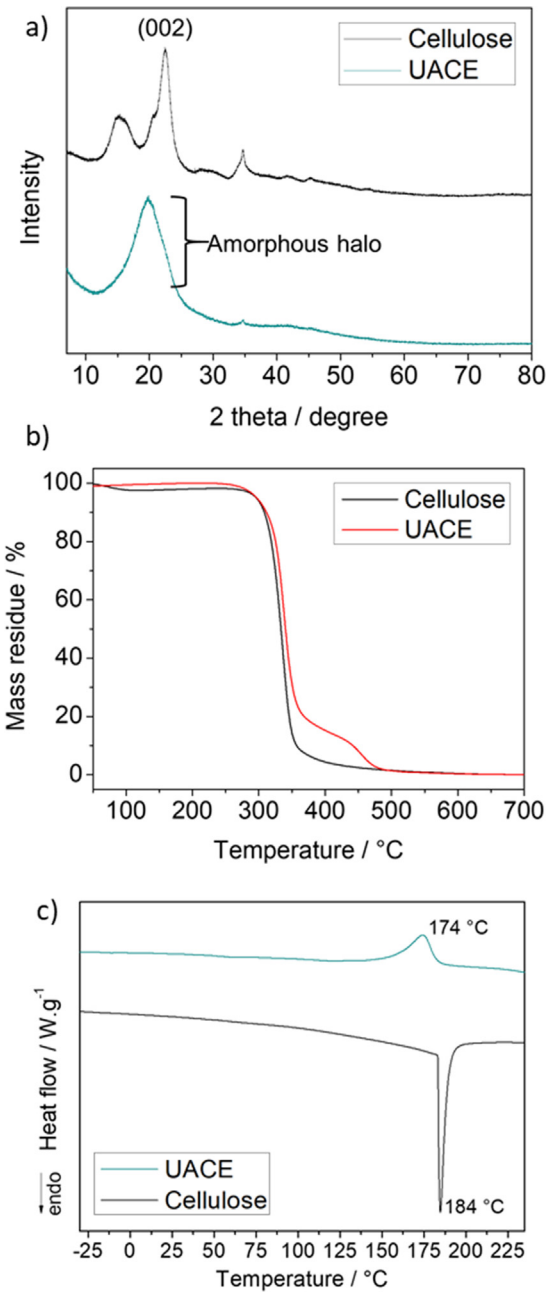

Fig. 2. a) X-rays diffractograms of native cellulose and udec-10-enoic acid cellulose esters, UACE. b) Thermogravimetric analyses of UACEs and their native cellulose precursors. c) Differential scanning calorimetry thermograms of cellulose and UACE.

improved mechanical properties, clean and environmentally harmless reaction, fast and regioselective polymerization, and degradability improvement that thiol-ene moieties can provide [23]. We used the bio-based dithiol crosslinker, DL-dithiothreitol, to cross-link UACE in miniemulsion and to form the cellulose-based nanocarriers (Fig. 3).

Captan and Pyraclostrobin were chosen as fungicides, which were encapsulated *in situ* into the cellulose nanocarriers (their chemical structures are shown in Fig. 3). Both fungicides are effective against trunk disease-promoting fungi, such as *Phaeominiella chlamydospore* [24] and *Neonectria ditissima* (syn. *Neonectria galligena*) [10], which are major responsible fungi for Esca and Canker.

Cellulose-based nanocarriers loaded with fungicides were prepared by dissolving UACE in chloroform containing the fungicides and dispersing the organic phase in water by high shear energy to produce the miniemulsion (Fig. 3a), followed by thiol-ene reaction (Fig. 3b). The miniemulsion/solvent evaporation process allows the formation of nanodroplets of pre-synthesized polymers, e.g. cellulose undecenoate, and a volatile solvent, chloroform. The cross-linking thiol-ene reaction occurs within these droplets followed by solvent evaporation to form the nanocarriers. Emulsification/solvent evaporation processes have been extensively used for preparing micro- and nanosized particles from a different synthetic and biobased polymers [25]. For an extensive description regarding the aspects that influence nanodroplet formation and nucleation mechanism we refer to early works [26,27].

After the reaction and solvent evaporation, some aggregates that might have been formed during the crosslinking reaction were filtered off. The final solid content of the dispersion was typically between 1.0 and 1.3 wt%. Solid nanocarriers with average particle sizes of 170–230 nm and PDI 0.11–0.14 were obtained for plain particles and particles loaded with 20 wt% of the fungicides, respectively (measured by DLS, Table 2). The ζ-potentials at pH 7 were found to be ca. – 50 mV, due to the presence of the anionic surfactant. The introduction of fungicides increased the solid content of the dispersed phase, which contributed to an increase in particle size [26,27]. Furthermore, the presence of the fungicide in the dispersed phase might impact the interplay between the interfacial tension of the two immiscible liquid phases, which might lead to the formation of larger particles at higher concentrations of the fungicide. When amounts of fungicide were further increased to 30 wt% (to UACE), the DLS measurements showed multimodal size distributions, indicating aggregation of the nanocarriers under these conditions.

Visualization of the nanocarriers by SEM proved the spherical morphology and showed diameters between ca. 150 and 250 nm, consistent with DLS measurements (Figure S7: plain nanocarriers - CNP 01, Figure S7a), NCs containing Captan (CNP 02, Figure S7b) and NCs containing Pyraclostrobin (CNP 03, Figure S7c). The freeze-dried nanocarriers were analyzed by DSC and revealed a glass transition of ca 55 °C (Figure S8).

FT-IR spectroscopy of the nanocarriers further proved the successful reaction of the olefinic double bonds (Fig. 4). The comparison between the different nanocarriers (CNP 01, 02, and 03) to the precursor (UACE) showed an increase in alkane vibrations at 2921 and 2851 cm^{-1} after the reaction – related to CH antisymmetric and symmetric stretches from CH_x-groups as double bonds had been converted into single bonds (Figure S9a, note: IR spectra were normalized to the C — O band from AGU at ca. 1050 cm^{-1}). Besides, the decrease of double bond vibrations can be observed by the decrease of the band at 907 cm^{-1} correspondents to CH_2

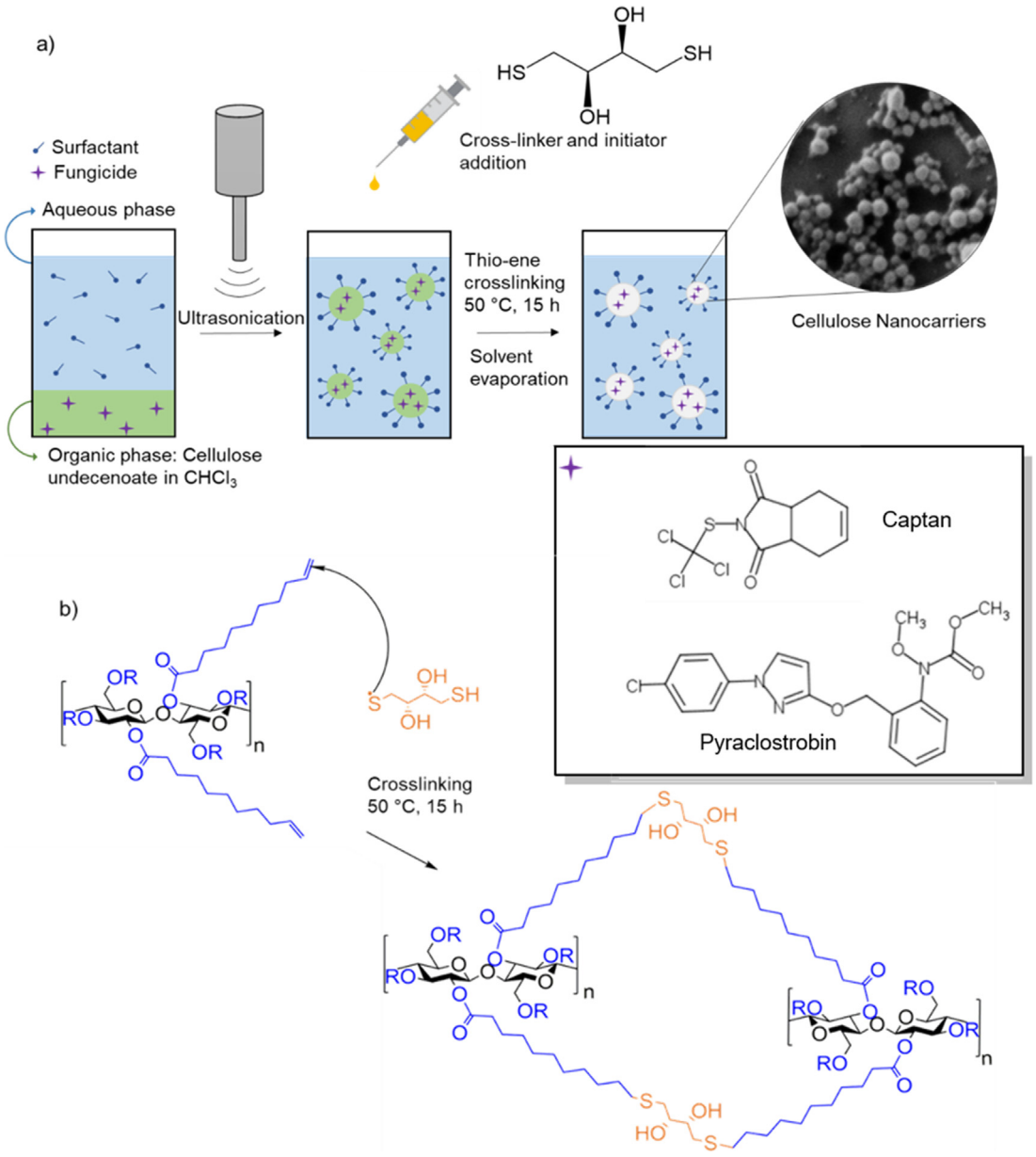

Fig. 3. a) Scheme of the preparation of cellulose-based nanocarriers, via thiol-ene addition in miniemulsion, loaded with fungicides as a potential drug delivery system in agriculture. Inset shows a respective SEM image of the nanocarriers (diameters ca. 200 nm). b) Scheme of the thiol-ene addition reaction to covalently crosslinked cellulose nanocarriers.

Table 2
Summary of cellulose-based nanocarriers containing captan and pyraclostrobin.

Entry	Fungicide	Load / mg·mL^{-1}	Dp / nm	PDI	ζ-potential / mV
CNP 01	–	–	167	0.12	− 54
CNP 02	Captan	2	230	0.11	− 48
CNP 03	Pyraclostrobin	2	222	0.14	− 49
CNP 04	Captan	3	228	0.44	–
CNP 05	Pyraclostrobin	3	324	0.64	–

out of plane wag in vinyl compounds, which is strongly present in the UACE precursor (Figure S9b). Moreover, –OH stretch bands at 3550 – 3400 cm^{-1} were detected in the crosslinked nanocarriers due to the presence of hydroxyls in the dithiol crosslinker. High encapsulation efficiencies (above 90%) of both captan (CNP02) and pyraclostrobin (CNP03) were determined by HPLC analyses (Fig. 5). The encapsulation efficiency was determined by analyzing the remaining concentration of fungicide in the supernatant after centrifugation (indirect method). In the case of captan (CNP02), no free fungicide was detected in the supernatant of duplicates, suggesting an almost quantitative encapsulation. When the encapsulation efficiency (EE) was determined by extraction of the fungicide from the nanocarriers (direct method), EE of 74 ± 29% was obtained (note: the considerable error is probably due to the diffi-

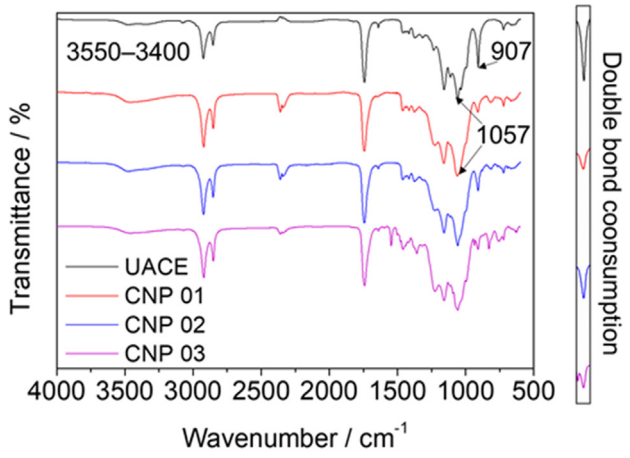

Fig. 4. FT-IR spectra of UACE and cellulose NCs, CNP 01, CNP 02 (captan 20 wt%) and CNP 03 (pyraclostrobin 20 wt%) after thiol-ene addition crosslinking in miniemulsion. By the side, the consumption of the double bond is shown.

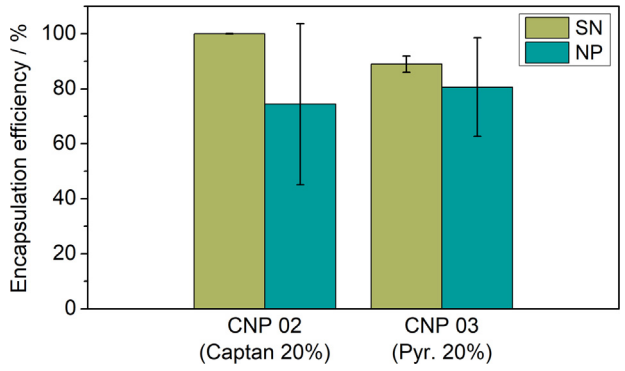

Fig. 5. Encapsulation efficiency of nanocarriers containing captan (CNP 02, 20 wt% to UACE or 2 mg·mL^{-1} in the dispersion) and pyraclostrobin (CNP 03, 20 wt% to UACE or 2 mg·mL^{-1} in the dispersion) determined by HPLC analysis of the supernatant (SN) or after extracting the encapsulated fungicide (NP). Error bars are the standard deviation of duplicates.

culty in extracting with THF from the crosslinked polymer matrix, but the average EE suggests a high loading efficiency during the crosslinking procedure). The EE of pyraclostrobin in CNP 03 measured indirectly from the supernatant of the duplicates was found to be 89 ± 3%, whereas the results based on the measurements of pyraclostrobin encapsulation obtained by its extraction from the nanocarriers revealed an EE of 81 ± 18%. Overall, miniemulsion crosslinking of UACE provided satisfactory results regarding the encapsulation of the agrochemicals captan and pyraclostrobin.

3.3. Antifungal activity

Antifungal activities *in vitro* were evaluated in terms of minimum inhibitory concentration (MIC) and inhibition of spore germination and fungal growth, respectively. Minimum inhibitory concentration is a dose-dependent antifungal activity assay and is considered the lowest concentration capable of inhibiting measurable growth. Nanoformulations CNP01 (empty nanocarriers), CNP02 (captan, 2 mg·mL^{-1}), CNP03 (pyraclostrobin, 2 mg·mL^{-1}), CNP04 (captan, 3 mg·mL^{-1}), CNP05 (pyraclostrobin, 3 mg·mL^{-1}) and the mixture CNP04/CNP05 were tested. The test organisms for the MIC assay *P. chlamydospore*, *N. ditissima, Phytophthora infestans, Magnaporthe oryzae, Botrytis cinereal,* and *Neofusicoccum parvum* segregate cellulases and should be capable of degrading the nanocarriers.

Botrytis cinerea is a necrotrophic fungus that causes grey mold in many plant species such as wines and strawberry.[28] *Magnaporthe oryzae* is a pathogenic fungus that causes mainly rice blast disease.[29] *Neofusicoccum parvum* is one of the most aggressive members of *Botryosphaeriaceae* and is related to canker pathology in fruit trees.[30] *Neonectria ditissima* (syn. *Neonectria galligena*) is a pathogen responsible for Apple Canker, a disease damaging the bark, leaves, and fruits and causing the death of seedlings and production losses.[11] *Phytophthora infestans* is an oomycete responsible for late blight, a very destructive disease in potato plants.[31] *Phaeomoniella. chlamydospore* is phytopathogenic fungus globally known to be related to trunk diseases in grapevines such as Esca disease and Petri disease.[32]

Nanoformulations were more efficient than the pyraclostrobin bulk formulation for the growth inhibition of standard organisms (Table 3), *P. infestans, M. oryzae* and *B. cinereal,* which are more susceptible than the Esca and apple canker pathogens. Nanoformulations present a high surface area and are water-dispersible which increases the availability of drugs in the growth medium promoting lower MICs, whereas bulk formulations are normally introduced with an amount of solvent such as ethanol to improve their solubility in the media. Even though fungicides concentration in the well was the same for all formulations, the increase of drug concentration within the nanocarrier, i.e. drug-to-UACE ratio, has successfully promoted lower MIC probably due to faster release. The combination of CNP04 and CNP05 was mostly not activity-enhancing, only in *Magnaporthe* a synergistic effect was visible. Empty cellulose nanocarriers, CNP 01, did not present activity towards fungal growth inhibition; it was able to inhibit the growth of *Magnaporthe* at the highest concentration; however, probably the amount of solvent (ethanol) used in the dilution was already enough to cause inhibition or, since *Magnaporthe* spores are quite sensitive, the rough surfaces produced by sedimenting particles could also trigger sporulation.

Phaeoacremonium minimum and *Neonectria ditissima*, related to severe trunk diseases, were chosen for spores germination and mycelial growth assays, in which growth of microorganisms was also determined by the OD at 600 nm (Fig. 6). Cellulose nanocarriers dispersions were incubated together with the spores and included hyphae for 96 h. Positive control consists of a spore and hyphae sample without nanocarriers, only growth medium, while the positive control consists of hygromycin at 100 μg·mL^{-1}. Captan was tested for comparison at 25 μg·mL^{-1}. The growth was normalized to the value relative to the positive control, which is considered 100% spore germination and mycelial growth. The fungal growth is displayed in Fig. 7 and the inhibition is considered as 100% minus the growth displayed in the graph. The results obtained for the empty cellulose NCs demonstrate that the NCs alone did not inhibit the growth of *N. ditissima*, quite the opposite, the presence of cellulose nanocarriers has allowed *N. ditissima* to grow past the positive control, probably because the nanocarriers are a source of nutrients. Interestingly, empty cellulose NCs have affected the growth of *P. minimum* by 15% inhibition. The negative control, hygromycin, has inhibited the spore germination and mycelial growth of *N. ditissima* and *P. minimum* by 80% and 95%, respectively. Plain captan has exhibited fungal growth inhibition of 70% for *N. ditissima* and of ca. 95% for P. minimum. During the *in vitro* tests conducted in 96-well plates for four days, and thereby an inoculation time twice as long as the duration of MIC tests, stronger inhibition of *N. ditissima* was observed. Therefore, we were able to show that captan has a higher effect on mycelial growths (*in vitro* tests) compared to spore germination (MIC tests).

Cellulose nanocarriers with different fungicide amounts were analyzed: CNP 02 containing captan 20 wt% or 2 mg·mL^{-1}; CNP 03 containing pyraclostrobin 20 wt% or 2 mg·mL^{-1}, CNP 04 containing captan 30 wt% or 3 mg·mL^{-1}, and CNP 05 containing pyra-

Table 3
Dose-dependent antifungal activities of NCs formulations and free fungicides. Minimum inhibitory concentration (MIC) towards *P. chlamydospore*, *N. ditissima*, *P. infestans*, *M. oryzae*, *B. cinereal*, and *Ne. parvum*. MIC (active ingredient, μg·mL^{-1}) represents the concentration at which inhibition of spore germination was first observed. Hygromycin and ciclopirox were used as positive controls for the MIC.

Formulations		Minimum inhibitory concentration / μg·mL^{-1}					
		P. infestans	*M. oryzae*	*B. cinerea*	*P. chlamydospora*	*N. ditissima*	*Ne. parvum*
CNP 01	(Empty)	>50	50	>50	>50	>50	>50
CNP 02	Cap.(20 wt%)	5–10	1–5	25	25	>50	>50
CNP 03	Pyr. (20 wt%)	>50	25	10	10	50	5
CNP 04	Cap. (30 wt%)	25	0.5	0.5	50	>50	>50
CNP 05	Pyr. (30 wt%)	25	5	5	10	50	5
CNP 04/05	Cap./Pyr.	10	0.5	10	25	>50	10
Pyraclostrobin		>50	10	10	10	50	5
Hygromycin		10	5	5	5	25	10
Ciclopirox		5	5	5	10	10	5

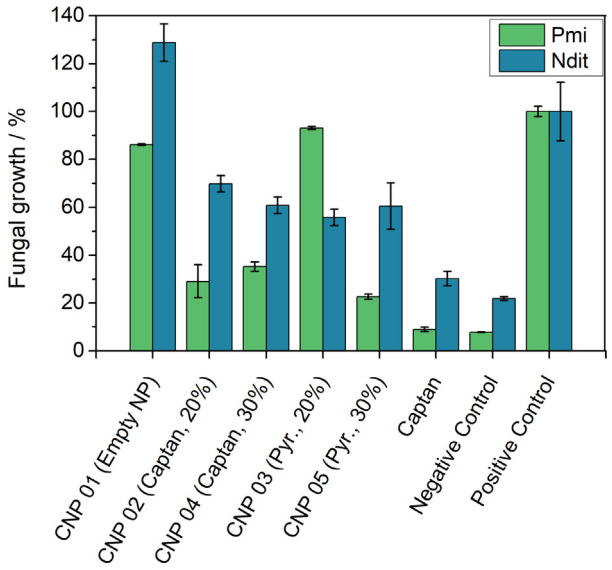

Fig. 6. *Phaeoacremonium minimum* (Pmi) and *Neonectria ditissima* (Ndit) spores germination and mycelial growth were determined by the optical density of the media at 600 nm. The nanocarriers dispersions were incubated together with the spores for 96 h. Positive control consists of a spore sample without nanocarriers, only water, while the negative control consists of hygromycin at 100 μg·mL^{-1}. Captan bulk formulation was tested for comparison at 25 μg·mL^{-1}. The growth was normalized to the value relative to the positive control, which is considered 100% spore germination and mycelial growth. Error bars are the standard deviation from triplicates.

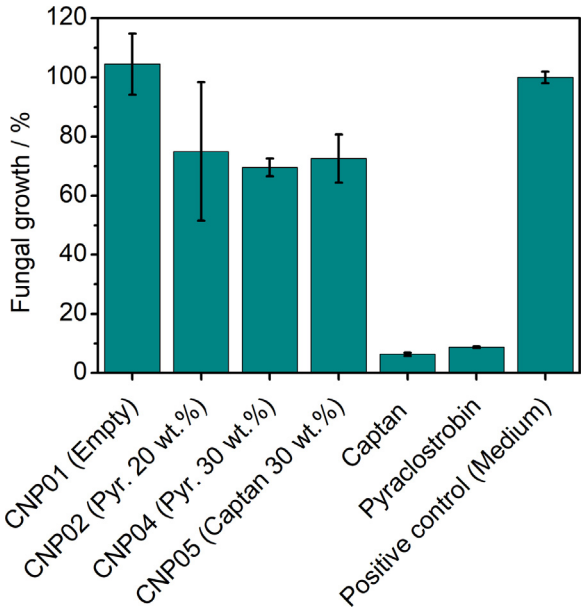

Fig. 7. *Cylindrocladium buxicola* spores germination and mycelial growth were determined by the optical density of the media (measured at 600 nm). The nanocarriers dispersions were incubated together with the spores for 96 h. The positive control consisted only of growth medium. The captan bulk formulation was tested at 25 μg·mL^{-1}. The growth was normalized to the value relative to the positive control, which was considered 100% spore germination and mycelial growth. Error bars are the standard deviation from triplicates.

clostrobin 30 wt% or 3 mg·mL^{-1}. Although the final concentration of fungicide in the well was kept the same, NCs with higher drug-load were expected to present an intensified activity due to the higher fungicide-to-nanoparticle weight ratio. Nevertheless, CNP 02 and CNP 04 presented similar performance towards the assays with inhibition of ca. 70% for *P. minimum* and of ca. 35% for *N. ditissima*. Their performance improved when analyzed in comparison to empty cellulose NCs. For CNP 01 a 120% growth of *N. ditissima* was detected compared to the control, which might be explained by the fact that the nanocarriers are nutrients to support fungal growth; whereas CNP 02 and 04 have allowed only 60 – 70% of growth; this is an improvement of ca. 50%. CNP 03 and CNP 05 presented a perceptible discrepancy in antifungal activity towards *P. minimum*, 10% and 80% of inhibition respectively, due to the concentration of drug inside the nanocarriers; once the release triggered by degradation, NCs enclosing a higher amount of fungicides establishes faster release kinetics. Whereas for *N. ditissima*, both CNP 03 and 05 allowed similar growth of 60%, i.e. 40% of inhibition. Finally, free captan and hygromycin had allowed very little growth due to their imminent availability, while NCs only release the active by diffusion or towards cellulolytic degradation. *In vitro* studies are the first step towards proceeding test systems such as *in vivo* and during field trials, which can provide more pieces of evidence to reinforce the applicability of NCs drug delivery systems in plants and their translation from *in vitro* assays to living organisms.

To underline the enzymatic release of the fungicides, we investigated their activity also against an organism that does not produce any cellulase. The enzymatic degradation of cellulose esters depends on a rather intricate synergy between different enzymes, e.g. esterases and cellulases/glucanases, especially for highly substituted cellulose esters, which has led several authors to use degradation protocols based on microorganisms.[33,34] Therefore, rather than using an artificial combination of enzymes, we decided to use fungi that could and could not degrade cellulose and compared the growth inhibition after fungicide release.

Nanocarriers loaded with captan and pyraclostrobin were submitted to *in vitro* tests with *Cylindrocladium buxicola* (Fig. 7). Bulk formulations of captan and pyraclostrobin were able to inhibit fungal growth by ca. 90% in comparison to the positive control, the

pure culture medium. In contrast, when the cellulose nanocarriers (not loaded with a drug) were administered to the spores, the optical density remained relatively unchanged. The drug-loaded cellulose nanocarriers (CNP02, 04, and 05) resulted in a slight decrease in the mycelial growth by 30%, which might be attributed to some drug leakage by diffusion under the conditions of the experiment. However, the inhibition of the mycelial growth of *Cylindrocladium buxicola* by the nanoformulations was much lower compared to the other investigated organisms (e.g. *P. minimum* and *N. ditissima)* that are capable of producing cellulose and thus degrading the nanocarriers.

4. Conclusion

This work presents a general approach for the delivery of agrochemicals mediated by NCs and triggered by cellulase-segregating pathogens, which are responsible for causing devastating fungal diseases in fruiting trees.

Cellulose was modified with undec-10-enoic acid, a compound derived from castor oil. Highly substituted cellulose fatty acid esters (UACE) were prepared with a DS of 2.35. The attachment of fatty acid residues to cellulose enabled the emulsification together with commercial hydrophobic fungicides (captan and pyraclostrobin), which are currently widely used in agriculture. After emulsification, we were able to prepare the first cross-linked and fungicide-loaded cellulose nanocarriers. Thiol-ene reaction with D,L-dithiothreitol produced nanocarriers loaded with up to 30 wt% of the drug and diameters between 150 and 250 nm. Captan and pyraclostrobin were encapsulated in high efficiencies (above 70%, determined by HPLC). The cellulose-based drug-loaded nanocarriers were able to efficiently inhibit the growth of several plant pathogens, such as *P. minimum* and *N. ditissima,* that release cellulases and are responsible for severe plant diseases (Esca a devastating grapevine trunk disease and European canker). Importantly, the drug-loaded nanocarriers were less efficient against *C. buxicola*, a microorganism that cannot produce cellulase, underlining the selective release of the cargo in the presence of cellulase that leads to enzymatic degradation of the cellulose matrix. In summary, we believe that our bio-based and biodegradable cellulose nanocarriers might be a promising platform to treat such severe plant diseases, which – to date – cannot be cured by conventional applications. However, trunk injection of the nanocarriers is a promising and environmentally friendly delivery method to reduce the amounts of fungicides and as a cure for these plant diseases, which is the subject of our further studies.

CRediT authorship contribution statement

Thiago O. Machado: Investigation, Methodology, Writing - original draft, Writing - review & editing. **Sebastian J. Beckers:** Investigation, Methodology, Writing - original draft, Writing - review & editing. **Jochen Fischer:** Investigation, Methodology, Writing - original draft, Writing - review & editing. **Claudia Sayer:** Supervision, Writing - review & editing. **Pedro H.H. de Araújo:** Supervision, Writing - review & editing. **Katharina Landfester:** Supervision, Writing - review & editing. **Frederik R. Wurm:** Conceptualization, Project administration, Funding acquisition, Supervision, Writing - review & editing.

Declaration of Competing Interest

The authors declare that they have no known competing financial interests or personal relationships that could have appeared to influence the work reported in this paper.

Acknowledgements

Parts of this research were supported by the Bio-Based Industries Joint Undertaking under the European Union's Horizon 2020 research and innovation program "BioRescue" (grant agreement no. 720708). We are also grateful to the Coordenação de Aperfeiçoamento de Pessoal de Nível Superior, CAPES, especially to the CAPES-PRINT Program (Project number 88887.310560/2018-00), and to the Conselho Nacional de Desenvolvimento Científico e Tecnológico, CNPq.

Appendix A. Supplementary material

Associated content

Supporting Information: Scheme of the UACE synthesis; SEM images; DSC curves; HPLC calibration curves and FT-IR spectra.

Supplementary data to this article can be found online at https://doi.org/10.1016/j.jcis.2021.05.030.

References

[1] X. Zhao, H. Cui, Y. Wang, C. Sun, B. Cui, Z. Zeng, Development Strategies and Prospects of Nano-Based Smart Pesticide Formulation, J. Agric. Food Chem. 66 (26) (2018) 6504–6512, https://doi.org/10.1021/acs.jafc.7b02004.

[2] M. Arias-Estévez, E. López-Periago, E. Martínez-Carballo, J. Simal-Gándara, J.C. Mejuto, L. García-Río, The Mobility and Degradation of Pesticides in Soils and the Pollution of Groundwater Resources, Agric. Ecosyst. Environ. 123 (4) (2008) 247–260, https://doi.org/10.1016/j.agee.2007.07.011.

[3] K. Fenner, S. Canonica, L.P. Wackett, M. Elsner, Evaluating Pesticide Degradation in the Environment: Blind Spots and Emerging Opportunities, Science (80-.) 341 (6147) (2013) 752–758, https://doi.org/10.1126/science.1236281.

[4] M. Lechenet, F. Dessaint, G. Py, D. Makowski, N. Munier-Jolain, Reducing Pesticide Use While Preserving Crop Productivity and Profitability on Arable Farms, Nat. Plants 3 (March) (2017) 1–6, https://doi.org/10.1038/nplants.2017.8.

[5] C. Parisi, M. Vigani, E. Rodríguez-Cerezo, Agricultural Nanotechnologies: What Are the Current Possibilities?, Nano Today 10 (2) (2015) 124–127, https://doi.org/10.1016/j.nantod.2014.09.009.

[6] S. Kumar, M. Nehra, N. Dilbaghi, G. Marrazza, A.A. Hassan, K.H. Kim, Nano-Based Smart Pesticide Formulations: Emerging Opportunities for Agriculture, J. Control. Release 2019 (294) (November 2018) 131–153, https://doi.org/10.1016/j.jconrel.2018.12.012.

[7] J. Fischer, S.J. Beckers, D. Yiamsawas, E. Thines, K. Landfester, F.R. Wurm, Targeted Drug Delivery in Plants: Enzyme-Responsive Lignin Nanocarriers for the Curative Treatment of the Worldwide Grapevine Trunk Disease Esca, Adv. Sci. 1802315 (2019), https://doi.org/10.1002/advs.201802315.

[8] T.O. Machado, S.J. Beckers, J. Fischer, B. Müller, C. Sayer, P.H.H. de Araújo, K. Landfester, F.R. Wurm, Bio-Based Lignin Nanocarriers Loaded with Fungicides as a Versatile Platform for Drug Delivery in Plants, Biomacromolecules 21 (7) (2020) 2755–2763, https://doi.org/10.1021/acs.biomac.0c00487.

[9] R.M. Beresford, K.S. Kim, Identification of Regional Climatic Conditions Favorable for Development of European Canker of Apple, Phytopathology 101 (1) (2011) 135–146, https://doi.org/10.1094/PHYTO-05-10-0137.

[10] R.W.S. Weber, Biologie Und Kontrolle Des Obstbaumkrebs-Erregers Neonectria Ditissima (Syn. N. Galligena) Aus Der Perspektive Nordwesteuropas, Erwerbs-Obstbau 56 (3) (2014) 95–107, https://doi.org/10.1007/s10341-014-0210-x.

[11] M. Wenneker, P.F. de Jong, N.N. Joosten, P.W. Goedhart, B.P.H.J. Thomma, Development of a Method for Detection of Latent European Fruit Tree Canker (Neonectria Ditissima) Infections in Apple and Pear Nurseries, Eur. J. Plant Pathol. 148 (3) (2017) 631–635, https://doi.org/10.1007/s10658-016-1115-3.

[12] S. Kumar, G. Bhanjana, A. Sharma, Sarita, M.C. Sidhu, N. Dilbaghi, Herbicide Loaded Carboxymethyl Cellulose Nanocapsules as Potential Carrier in Agrinanotechnology, Sci. Adv. Mater. 7 (6) (2015) 1143–1148, https://doi.org/10.1166/sam.2015.2243.

[13] Z. Söyler, M.A.R. Meier, Sustainable Functionalization of Cellulose and Starch with Diallyl Carbonate in Ionic Liquids, Green Chem. 19 (16) (2017) 3899–3907, https://doi.org/10.1039/C7GC01978E.

[14] S.R. Labafzadeh, K.J. Helminen, I. Kilpeläinen, A.W.T. King, Synthesis of Cellulose Methylcarbonate in Ionic Liquids Using Dimethylcarbonate, ChemSusChem 8 (1) (2015) 77–81, https://doi.org/10.1002/cssc.201402794.

[15] A. Schenzel, A. Hufendiek, C. Barner-Kowollik, M.A.R. Meier, Catalytic Transesterification of Cellulose in Ionic Liquids: Sustainable Access to Cellulose Esters, Green Chem. 16 (6) (2014) 3266, https://doi.org/10.1039/c4gc00312h.

[16] P.A. Fokou, M.A.R. Meier, Use of a Renewable and Degradable Monomer to Study the Temperature-Dependent Olefin Isomerization during ADMET Polymerizations, J. Am. Chem. Soc. 131 (5) (2009) 1664–1665, https://doi.org/10.1021/ja808679w.

[17] A.W.T. King, J. Jalomäki, M. Granström, D.S. Argyropoulos, S. Heikkinen, I. Kilpeläinen, A New Method for Rapid Degree of Substitution and Purity Determination of Chloroform-Soluble Cellulose Esters, Using 31P NMR, Anal. Methods 2 (10) (2010) 1499–1505, https://doi.org/10.1039/c0ay00336k.
[18] U.P. Agarwal, R.R. Reiner, S.A. Ralph, Estimation of Cellulose Crystallinity of Lignocelluloses Using Near-IR, J. Agric. Food Chem. 61 (2013) 103–113, https://doi.org/10.1021/jf304465k.
[19] K.N. Onwukamike, S. Grelier, E. Grau, H. Cramail, M.A.R. Meier, Sustainable Transesterification of Cellulose with High Oleic Sunflower Oil in a DBU-CO 2 Switchable Solvent, ACS Sustain. Chem. Eng. 6 (7) (2018) 8826–8835, https://doi.org/10.1021/acssuschemeng.8b01186.
[20] E. Piorkowska, G.C. Rutledge, Handbook of Polymer Crystallization (2013), https://doi.org/10.1002/9781118541838.
[21] G. Thoorens, F. Krier, B. Leclercq, B. Carlin, B. Evrard, Microcrystalline Cellulose, a Direct Compression Binder in a Quality by Design Environment - A Review, Int. J. Pharm. 473 (1–2) (2014) 64–72, https://doi.org/10.1016/j.ijpharm.2014.06.055.
[22] P.B. Cardoso, T.O. Machado, P.E. Feuser, C. Sayer, M.A.R. Meier, P.H.H. Araújo, Biocompatible Polymeric Nanoparticles From Castor Oil Derivatives via Thiol-Ene Miniemulsion Polymerization, Eur. J. Lipid Sci. Technol. 1700212 (2017) 1700212, https://doi.org/10.1002/ejlt.201700212.
[23] T.O. Machado, C. Sayer, P.H.H. Araujo, Thiol-Ene Polymerisation: A Promising Technique to Obtain Novel Biomaterials, Eur. Polym. J. 86 (2017) 200–215, https://doi.org/10.1016/j.eurpolymj.2016.02.025.
[24] P.H. Fourie, F. Halleen, Chemical and Biological Protection of Grapevine Propagation Material from Trunk Disease Pathogens, Eur. J. Plant Pathol. 116 (4) (2006) 255–265, https://doi.org/10.1007/s10658-006-9057-9.
[25] R.H. Staff, K. Landfester, D. Crespy, Recent Advances in the Emulsion Solvent Evaporation Technique for the Preparation of Nanoparticles and Nanocapsules, Adv. Polym. Sci. 262 (October) (2013) 329–344, https://doi.org/10.1007/12_2013_233.
[26] A. Musyanovych, J. Schmitz-Wienke, V. Mailänder, P. Walther, K. Landfester, Preparation of Biodegradable Polymer Nanoparticles by Miniemulsion Technique and Their Cell Interactions, Macromol. Biosci. 8 (2) (2008) 127–139, https://doi.org/10.1002/mabi.200700241.
[27] R.H. Staff, D. Schaeffel, A. Turshatov, D. Donadio, H.J. Butt, K. Landfester, K. Koynov, D. Crespy, Particle Formation in the Emulsion-Solvent Evaporation Process, Small 9 (20) (2013) 3514–3522, https://doi.org/10.1002/smll.201300372.
[28] B. Williamson, B. Tudzynski, P. Tudzynski, J.A.L. Van Kan, Botrytis Cinerea: The Cause of Grey Mould Disease, Mol. Plant Pathol. 8 (5) (2007) 561–580, https://doi.org/10.1111/j.1364-3703.2007.00417.x.
[29] R.A. Wilson, N.J. Talbot, Under Pressure: Investigating the Biology of Plant Infection by Magnaporthe Oryzae, Nat. Rev. Microbiol. 7 (3) (2009) 185–195, https://doi.org/10.1038/nrmicro2032.
[30] E. Iturritxa, B. Slippers, N. Mesanza, M.J. Wingfield, First Report of Neofusicoccum Parvum Causing Canker and Die-Back of Eucalyptus in Spain, Australas. Plant Dis. Notes 6 (1) (2011) 57–59, https://doi.org/10.1007/s13314-011-0019-5.
[31] S. Maurice, M.S. Montes, B.J. Nielsen, L. Bødker, M.D. Martin, C.G. Jønck, R. Kjøller, S. Rosendahl, Population Genomics of an Outbreak of the Potato Late Blight Pathogen, Phytophthora Infestans, Reveals Both Clonality and High Genotypic Diversity, Mol. Plant Pathol. 20 (8) (2019) 1134–1146, https://doi.org/10.1111/mpp.12819.
[32] P.S.R. Vergaças, A.B.M. Ferreira, D.A. de S. Franco, L.G. Leite, W.N. Campos, R. Harakava, C. Bueno Júnior, Survey of Phaeomoniella Chlamydospora in Vineyard Weeds, Summa Phytopathol. 44 (3) (2018) 218–222, https://doi.org/10.1590/0100-5405/180135.
[33] J. Puls, S.A. Wilson, D. Hölter, Degradation of Cellulose Acetate-Based Materials: A Review, J. Polym. Environ. 19 (1) (2011) 152–165, https://doi.org/10.1007/s10924-010-0258-0.
[34] N. Yadav, M. Hakkarainen, Degradable or Not? Cellulose Acetate as a Model for Complicated Interplay between Structure, Environment and Degradation. *Chemosphere* 265 (2021), https://doi.org/10.1016/j.chemosphere.2020.128731 128731.